probed with fluorescein-conjugated secondary antibodies (1:100 dilution; Jackson ImmunoResearch Labs) and rhodamine-phalloidin (0.66 μM; Molecular Probes). Immunostaining after microinjection of MG-labeled antibodies (1 mg/ml) into neurons with or without fluorescent dextran marker was done by directly incubating with fluorescent secondary antibody. Images were taken with a Zeiss LSM 410 confocal microscope equipped with a 63× plan-Apochromat [numerical aperture (NA) = 1.4] oil-immersion lens.

15. D. G. Jay, *Proc. Natl. Acad. Sci. U.S.A.* **85**, 5454 (1988). All antibodies were labeled with MG to the same ratios (6 to 9 dyes per IgG molecule).
16. Sliding actin filament assay was done essentially as described (*13*). Briefly, myosin-V (25 μg/ml) was perfused into motility chambers and allowed to absorb onto the nitrocellulose cover slips for 10 min. After rinses with blocking buffer to remove unbound myosins, MG-labeled antibodies (47.5 μg/ml; molar ratio myosin-V:IgG = 1:7) were added to the chamber and incubated for 30 min. After the removal of unbound antibodies, half of the motility chambers were marked with ink and subjected to laser irradiation for 5 min. After the addition and examination of actin filaments (rhodamine-phalloidin F-actin; 12 nM) in the absence of ATP, sliding was initiated by the addition of motility buffer containing 2 mM ATP. The density of bound actin filaments was indistinguishable between laser-irradiated and unirradiated areas before the initiation of motility. After the addition of ATP, most of the filaments inside the irradiated area were released intact, although a few exhibited Brownian motion and detached gradually. Motility was recorded with a Nikon Diaphot 300 microscope equipped with epifluorescence optics (Plan Apo 100× NA 1.4 oil-immersion objective) and a Dage-MTI SIT camera. Time-lapse images were digitized with MetaMorph image acquisition software (Universal Images, PA) and then transferred to an optical laser disc recorder. Motility assays were done at 24° ± 1°C. A yttrium-aluminum-garnet–Nd (YAG-Nd)–pumped dye laser (models GCR11 and PDL2, Spectra Physics) was used to generate a 620-nm light at an energy output of 18 mJ per pulse (2-mm-diameter laser spot).
17. Chick brain myosin-V was purified and Mg^{2+}ATPase assays were done as described (*8*). Samples contained a final concentration of 4.5 μg/ml myosin-V, 860 μg/ml F-actin, and 430 μg/ml calmodulin. Aliquots were incubated for 0 or 7 min at 37°C in ATPase buffer. For CALI assays, myosin-V was incubated with either MG–anti-MV or MG-IgG (molar ratio myosin-V:IgG = 1:7) for 30 min and then laser-irradiated for 5 min before assessment with ATPase assay (*16*). Laser irradiation of purified myosin-V in solution had no effect on the actin-activated Mg^{2+}-ATPase activity of myosin-V (24.70 ± 0.10 versus 27.15 ± 0.75 without irradiation). Further, CALI did not inhibit myosin-V ATPase activity in the presence of MG–anti-MV (16.80 ± 2.00 versus 16.95 ± 2.95 without irradiation) or MG-IgG (17.95 ± 2.95 versus 18.40 ± 1.00 without irradiation). Results are the averages ± SEM from three independent assays. ATPase activities are given in ATP molecules per myosin-V head per second.
18. Chick DRG cultures were maintained at 37°C on the microscope stage with a stage incubator. MG-labeled antibodies mixed with fluorescein-dextran (3 mg/ml; Molecular Probes) were microinjected into neurons. After a 30- to 60-min incubation, healthy neurons were selected for micro-CALI experiments (*11*). A selected area of the growth cone was observed for 5 min, subjected to laser irradiation for 5 min, and followed for an additional 10-min examination with a Zeiss Axiovert 10 microscope with phase-contrast optics. Time-lapse images (one frame every 15 s) and image enhancements were facilitated by custom-written software and recorded on an optical laser disc recorder (*11*). The laser beam for micro-CALI was generated with a nitrogen-pumped dye laser (model VSL-337, Laser Science) at an energy output of 30 μJ per pulse (10-μm-diameter laser spot).
19. A. M. Sydor, A. Su, F.-S. Wang, A. Xu, D. G. Jay, *J. Cell Biol.*, in press.
20. B. Barylko, M. C. Wagner, O. Reizes, J. P. Albanesi, *Proc. Natl. Acad. Sci. U.S.A.* **89**, 490 (1992); M. C. Wagner, B. Barylko, J. P. Albanesi, *J. Cell Biol.* **119**, 163 (1992).
21. M. L. Springer, B. Patterson, J. A. Spudich, *Development* **120**, 2651 (1994).
22. B. Govindan, R. Bowser, P. Novick, *J. Cell Biol.* **128**, 1055 (1995); G. Jung and J. Hammer, *ibid.* **110**, 1955 (1990); J. A. Mercer, P. K. Seperack, M. C. Strobel, N. G. Copeland, N. A. Jenkins, *Nature* **349**, 709 (1991); K. Novak and M. Titus, *Mol. Biol. Cell* **3**, 3a (1992); V. R. Simon, T. C. Swayne, L. A. Pon, *J. Cell Biol.* **130**, 345 (1995); M. A. Titus, D. Wessels, J. A. Spudich, D. Soll, *Mol. Biol. Cell* **4**, 233 (1993).
23. H. M. Buettner, R. N. Pittman, J. K. Ivins, *Dev. Biol.* **163**, 407 (1994).
24. We thank A. Xu for technical assistance and J. P. Albanesi (University of Texas Southwestern Medical Center, Dallas) for providing monoclonal antibodies to myosin-Iβ (M2 and M3). Supported in part by National Institutes of Health (NIH) grants NS-29007 and NS-34699 (to D.G.J.) and DK-25387 (to M.S.M.), the Lucille P. Markey Charitable Trust and Klingenstein fellowship (to D.G.J.), and the Pew Charitable Trust (to J.S.W.). F.-S.W. acknowledges receipt of a postdoctoral fellowship from the NIH.

15 January 1996; accepted 20 May 1996

PTH/PTHrP Receptor in Early Development and Indian Hedgehog–Regulated Bone Growth

Beate Lanske, Andrew C. Karaplis, Kaechong Lee, Arne Luz, Andrea Vortkamp, Alison Pirro, Marcel Karperien, Libert H. K. Defize, Chrystal Ho, Richard C. Mulligan, Abdul-Badi Abou-Samra, Harald Jüppner, Gino V. Segre, Henry M. Kronenberg*

The PTH/PTHrP receptor binds to two ligands with distinct functions: the calcium-regulating hormone, parathyroid hormone (PTH), and the paracrine factor, PTH-related protein (PTHrP). Each ligand, in turn, is likely to activate more than one receptor. The functions of the PTH/PTHrP receptor were investigated by deletion of the murine gene by homologous recombination. Most PTH/PTHrP receptor (−/−) mutant mice died in mid-gestation, a phenotype not observed in PTHrP (−/−) mice, perhaps because of the effects of maternal PTHrP. Mice that survived exhibited accelerated differentiation of chondrocytes in bone, and their bones, grown in explant culture, were resistant to the effects of PTHrP and Sonic hedgehog. These results suggest that the PTH/PTHrP receptor mediates the effects of Indian Hedgehog and PTHrP on chondrocyte differentiation.

The PTH/PTHrP receptor responds to two ligands, PTH and PTHrP. PTH is synthesized by the parathyroid glands and acts on kidney and bone to regulate calcium homeostasis (*1*). PTHrP, in contrast, is synthesized in multiple tissues with specific spatial and temporal profiles and has largely paracrine functions (*2*).

Complementary DNA encoding the PTH/PTHrP receptor was cloned from bone and kidney cells. The receptor binds and responds equally to NH_2-terminal fragments of PTH and PTHrP (*3*, *4*). The PTH/PTHrP receptor mRNA is expressed in the PTH target organs, kidney and bone (*5*, *6*), as well as in organs in which PTHrP is expressed, such as extraembryonic membranes and growth plates of bone (*7*, *8*). Physiologic studies suggest that other receptors for PTH and PTHrP exist (*9*–*11*), one of which has been cloned (*12*).

At implantation, the murine PTH/PTHrP receptor is expressed in parietal endoderm immediately adjacent to PTHrP-expressing trophoblastic cells (*7*, *13*). Trophoblastic PTHrP induces the differentiation of the parietal endoderm and the subsequent synthesis of components of Reichert's membrane in vitro (*13*). Nevertheless, mice homozygous for a targeted deletion of PTHrP are normal early in development (*14*) and later manifest only abnormalities in endochondral bone development, and then die at birth.

Chondrocytes in the growth regions of bones of PTHrP (−/−) mice undergo fewer rounds of proliferation than in normal mice and differentiate prematurely into hypertrophic chondrocytes (*14*, *15*). In contrast, bone explants exposed to PTHrP NH_2-terminal fragment have delayed differentiation of hypertrophic chondrocytes (*16*).

B. Lanske, K. Lee, A. Pirro, A.-B. Abou-Samra, H. Jüppner, G. V. Segre, H. M. Kronenberg, Endocrine Unit, Massachusetts General Hospital and Harvard Medical School, Boston, MA 02114, USA.
A. C. Karaplis, Department of Medicine, Sir Mortimer B. Davis–Jewish General Hospital, McGill University, Montreal, Quebec H3T 1E2, Canada.
A. Luz, Institute of Pathology, GSF München, D 85758 Neuherberg, Germany.
A. Vortkamp, Department of Genetics, Harvard Medical School, Boston, MA 02115, USA.
M. Karperien and L. H. K. Defize, Hubrecht Laboratorium, Netherlands Institute for Developmental Biology, 3584 CT Utrecht, The Netherlands.
C. Ho, Department of Genetics and Howard Hughes Medical Institute, Harvard Medical School, Boston, MA 02115, USA.
R. C. Mulligan, Whitehead Institute for Biomedical Research, Cambridge, MA 02142, and Massachusetts Institute of Technology, Cambridge, MA 02139, USA.
*To whom correspondence should be addressed.

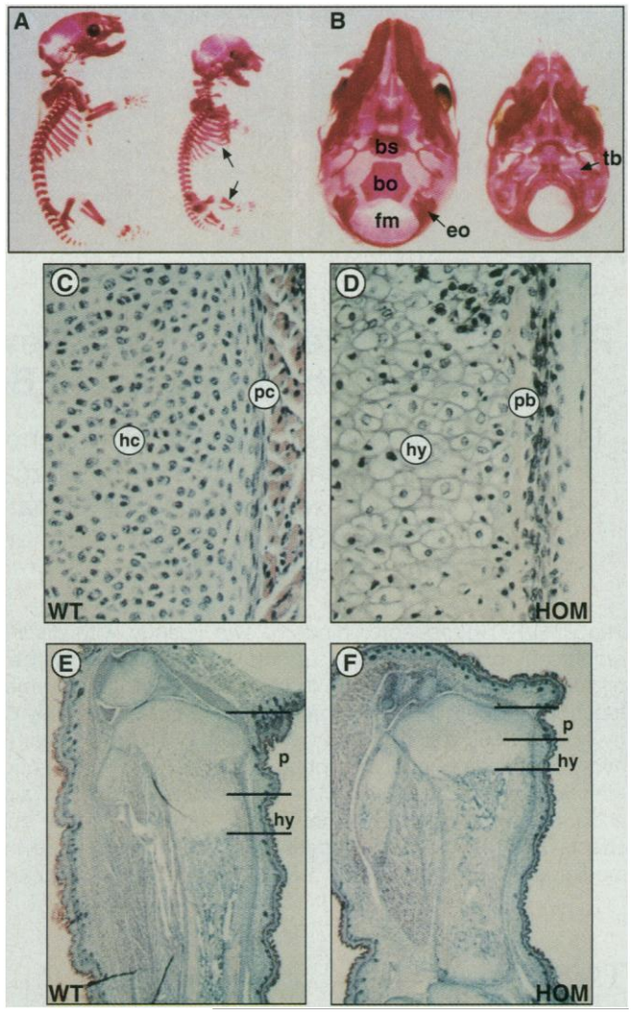

Fig. 1. Abnormalities in endochondral bone formation. (**A**) Lateral view of an entire skeleton after Alizarin red S staining of a wild-type (left) and a mutant (right) PTH/PTHrP receptor embryo at day 18.5 of gestation. Abnormalities in the mutant are apparent throughout the whole skeleton: for example, reduced size of the total skeleton, domed skull, and foreshortened mandible. Arrow (up) points to the abnormal mineralization of the sternum and ribs and indicates the lack of unmineralized cartilaginous tissue; arrow (down) points to the shortened long bones of the mutant. (**B**) Caudal view on the base of the skull (wild type, left; mutant, right). The Alizarin red S stain reveals excessive mineralization and therefore a synchondrosis between the basioccipital (bo), exoccipital (eo), and basisphenoid (bs). Narrowing of the foramen magnum (fm) and mineralized tympanic bulla (tb) are also apparent. Histological evaluation at the level of the fifth rib of a wild type (**C**) and mutant (**D**) at day 18.5 of gestation. The quiescent hyaline cartilage (hc) in the wild type is surrounded by perichondrium (pc), whereas the mutant cartilage is composed of hypertrophic chondrocytes (hy), surrounded by perichondrial bone (pb). Examination of the growth plate of the proximal tibia by light microscopy revealed marked anomalies in the homozygous (**F**) compared with the normal littermate (**E**), including a marked reduction in the zone of proliferating cartilage (p) and irregular and shorter columns of proliferating chondrocytes.

Table 1. Survival of homozygous offspring (−/−) in different genetic backgrounds. Heterozygous mice of the respective strain were interbred to obtain mice homozygous for the PTH/PTHrP receptor gene deletion. Cesarean section at the indicated day of gestation was carried out, and genotyping of the embryos was performed with Southern (DNA) blot analysis. From the first 10 litters of each group, all embryos were analyzed to confirm the expected pattern of Mendelian inheritance for wild-type and heterozygous mice. Because survival of wild-type and heterozygous animals was similar, we limited our studies to the homozygous mutants. Noninformative (Non-inf.) cases represent degenerated embryos that yielded insufficient DNA for analysis.

Genetic background	Days of gestation	No. in litter	Total no. of embryos	Alive (−/−) (%)	Dead (−/−) (%)	Non-inf. (%)
C57BL/6-129/SvJ	E9.5	19	153	33 (22)	3 (2)	12 (8)
C57BL/6-129/SvJ	E12.5	10	93	9 (10)	5 (5)	11 (12)
C57BL/6-129/SvJ	E14.5	10	69	3 (4)	8 (12)	4 (6)
C57BL/6-129/SvJ	E18.5	20	124	4 (3)	4 (3)	10 (8)
C57BL/6 (2nd backcross)	E18.5	22	168	4 (2)	4 (2)	0 (0)
MF-1 (3rd backcross)	E18.5	40	371	9 (2)	19 (4)	6 (2)
Black Swiss (1st backcross)	E18.5	56	434	51 (12)	25 (6)	9 (2)

Taken together, these data suggest that PTHrP delays chondrocyte differentiation, thereby allowing more chondrocyte proliferation. The accompanying research article (*16*) demonstrates that Indian hedgehog (Ihh), made by prehypertrophic and hypertrophic chondrocytes, also delays the differentiation of early hypertrophic chondrocytes in a negative feedback loop. Ihh stimulates the synthesis of PTHrP in perichondrial cells near the ends of long bones. The PTH/PTHrP receptor is expressed in prehypertrophic and hypertrophic chondrocytes and, to a lesser extent, in proliferating chondrocytes and is thus a candidate mediator of the PTHrP signal in the feedback loop that controls the rate and sites of chondrocyte differentiation (*8*). To establish the physiologic role of the cloned PTH/PTHrP receptor in the growth plate and to further explore the role of PTHrP in early development, we examined the phenotypes of mice homozygous for the ablation of the PTH/PTHrP receptor gene.

Gene targeting in embryonic stem (ES) cells was used to delete exons E2 through T, which encode most of the PTH/PTHrP receptor (*17*, *18*). Mice heterozygous for the PTH/PTHrP receptor gene deletion grew normally and were fertile. Mice homozygous for the PTH/PTHrP receptor gene deletion were smaller than normal from at least embryonic day 9.5 (E9.5) of fetal life (*19*). Histologic evaluation at E9.5 and E12.5 revealed morphologically normal development except for proportional diminution of organ size (*19*). Although the number of PTH/PTHrP receptor (−/−) fetuses met Mendelian expectations at E9.5, only 10% of the living fetuses were PTH/PTHrP receptor (−/−) at E12.5, and almost all these fetuses had died by E14.5 (Table 1). Because the only sites of synthesis of PTHrP and the PTH/PTHrP receptor before E9.5 are in extraembryonic membranes, Reichert's membrane and the parietal endoderm were examined (*7*, *13*), but no abnormalities in the morphology of Reichert's membrane or α-laminin staining were noted (*19*, *20*). Thus, the small size and early death of the PTH/PTHrP receptor (−/−) animals remains unexplained and contrasts with the normal phenotype of PTHrP (−/−) mice during early gestation. Maternal PTHrP—synthesized in large amounts by maternal cells in the decidua, located in the inner zone directly adjacent to the embryo (*21*, *22*)—may complement the absence of fetal PTHrP in the PTHrP (−/−) mice but not the absence of the fetal PTH/PTHrP receptor.

To search for genetic backgrounds that might allow evaluation of older fetuses, we backcrossed heterozygous mice of C57BL/6-129/SvJ background into different mouse strains. Only crosses with the Black Swiss

strain (Table 1) increased the survival of PTH/PTHrP receptor (−/−) embryos until birth. Although the Black Swiss background partially suppressed the early death phenotype, in all genetic backgrounds the PTH/PTHrP receptor (−/−) mice were proportionally smaller than normal. If allowed to complete gestation, all PTH/PTHrP receptor (−/−) animals died within a few minutes of birth. The appearance of the PTH/PTHrP receptor (−/−) animals at E18.5 of gestation was similar to that of the PTHrP (−/−) mice, in that they exhibited a domed skull, short snout and mandible, protruding tongue, and disproportionately short limbs (Fig. 1A) (*14*). Alizarin Red S staining (*23*) of skeletons of PTH/PTHrP receptor (−/−) mice revealed inappropriately accelerated mineralization exclusively of bones formed by endochondral replacement (Fig. 1, A and B).

Histological examinations of 18.5-day-old PTH/PTHrP receptor (−/−) fetuses (*24*) revealed a phenotype similar to that observed in the PTHrP (−/−) animals, in that the hyaline cartilage in the ribs adjacent to the sternum was differentiated into hypertrophic cartilage surrounded by prematurely mineralized osteoid matrix and active osteoblasts (Fig. 1, C and D) (*14*). The growth plate of the proximal tibia, like that of the PTHrP (−/−) fetuses, revealed irregular and markedly short columns of proliferating chondrocytes (Fig. 1, E and F). The similarities between the phenotypes of PTHrP (−/−) and PTH/PTHrP receptor (−/−) mice suggest that the PTH/PTHrP receptor mediates the actions of PTHrP on chondrocytes. This hypothesis is further supported by the presentation of humans with Jansen osteochondrodystrophy. These patients, with activating point mutations of the PTH/PTHrP receptor, exhibit growth plate abnormalities similar to those seen in the murine growth plate explants exposed to excess PTHrP (*25*). Our results support the hypothesis that this pathology reflects inappropriate PTHrP-like, but ligand-independent, activation of the PTH/PTHrP receptor.

In the accompanying research article (*16*), Ihh and PTHrP are shown to participate in a feedback loop that controls the pace of differentiation in the chicken and murine growth plates. To verify that the PTH/PTHrP receptor, which is expressed in a region that overlaps that of Ihh expression (Fig. 2, A to D) (*16*), mediates the actions of PTHrP in this feedback loop, we treated lower limb explants from PTH/PTHrP receptor (−/−) E16.5 fetal mice with PTHrP, with partially purified Sonic helgehog (Shh) (the actions of which resemble those of Ihh on the growth plate), or with control media (*26*). Treatment with control media showed that chondrocytes in PTH/PTHrP receptor (−/−) limbs became hypertrophic more rapidly in culture and expressed more type X collagen mRNA than those in normal limbs (Fig. 3, A and D), consistent with the hypothesis that the PTH/PTHrP receptor regulates the rate of hypertrophic conversion. Whereas in normal limbs, addition of either PTHrP or Shh resulted in expansion of the less differentiated chondrocyte population and suppression of differentiation into hypertrophic, type X collagen–producing chondrocytes (Fig. 3, B and C), neither PTHrP nor Shh had any effect on limbs from PTH/PTHrP receptor (−/−) fetuses (Fig. 3, E and F). This result supports those obtained with PTHrP (−/−) explants and suggests that PTH/PTHrP receptor–expressing chondrocytes are the targets of PTHrP in this pathway (*16*).

Our results, which show that neither Shh nor PTHrP slows differentiation of chondrocytes in bone explants of PTH/PTHrP receptor (−/−) limbs, establish that PTH/PTHrP receptor–expressing chondrocytes are the relevant physiologic target of the Ihh/PTHrP pathway. In the absence of PTH/PTHrP receptors, Ihh expression is

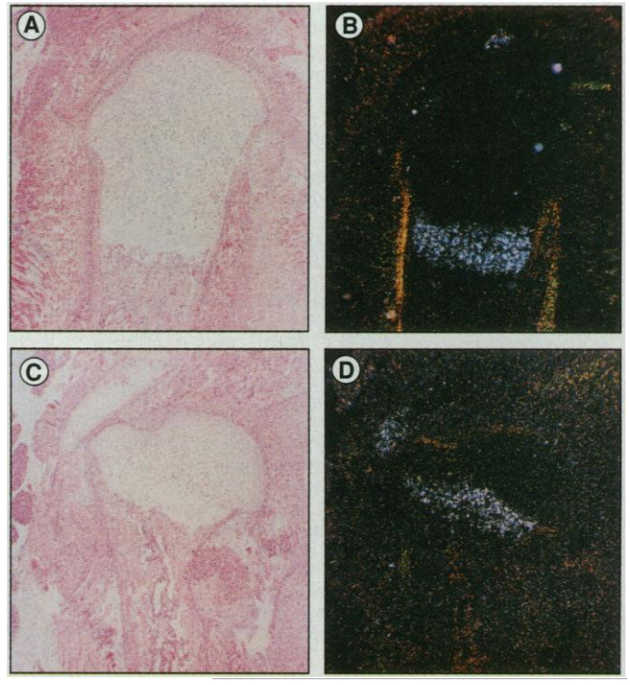

Fig. 2. Ihh mRNA expression in the humerus of E18.5 mouse embryos. In both wild-type (**A**, bright field; **B**, dark field) and mutant PTH/PTHrP receptor (−/−) fetuses (**C**, bright field; **D**,dark field), Ihh mRNA is expressed in prehypertrophic and hypertrophic chondrocytes, in a manner similar to its expression in chicken limbs (*16*). This pattern of expression is unchanged in the PTH/PTHrP receptor (−/−) embryos, although the cells expressing Ihh are nearer the articular end of the bone in mutant than in normal embryos. The yellow staining in the periosteum is an artifact (B).

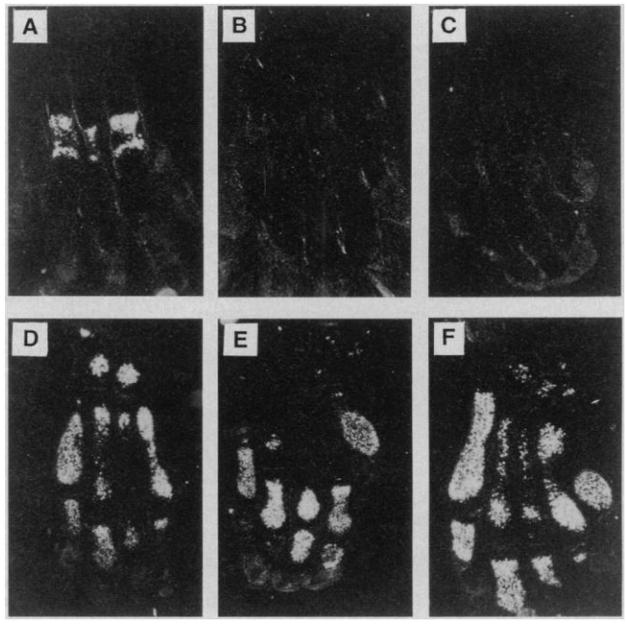

Fig. 3. Null response of PTH/PTHrP receptor (−/−) cartilage to PTHrP and Shh. E16.5 hind limbs from normal (**A** to **C**) and PTH/PTHrP receptor (−/−) mice (**D** to **F**) were cultured and treated with 10^{-7} M PTHrP (B and E), recombinant Shh (5 μg/ml) (C and F), or vehicle (A and D). Chondrocytic differentiation was assessed by type X collagen mRNA expression. PTH/PTHrP receptor (−/−) explants exhibited substantially advanced chondrocytic differentiation in vitro (D) compared with normal littermates (A). Whereas PTHrP or Shh suppressed hypertrophic differentiation in normal cartilage (B and C), neither had any effect on PTH/PTHrP receptor (−/−) cartilage (E and F).

found in cells much closer to the articular surface than normal. We conclude that Ihh, produced by differentiating chondrocytes, delays the differentiation of growth plate chondrocytes by stimulating the synthesis of perichondrial PTHrP, which then acts on the PTH/PTHrP receptor on chondrocytes.

REFERENCES AND NOTES

1. J. Potts Jr. *et al.*, in *Endocrinology*, L. DeGroot, Ed. (Saunders, Philadelphia, 1995), vol. 2, pp. 920–966.
2. A. E. Broadus and A. F. Stewart, in *The Parathyroids. Basic and Clinical Concepts*, J. P. Bilezikian, M. A. Levine, R. Marcus, Eds. (Raven, New York, 1994), pp. 259–294.
3. H. Jüppner *et al.*, *Science* **254**, 1024 (1991).
4. A. B. Abou-Samra *et al.*, *Proc. Natl. Acad. Sci. U.S.A.* **89**, 2732 (1992).
5. P. Ureña *et al.*, *Endocrinology* **133**, 617 (1993).
6. J. Tian, M. Smorgorzewski, L. Kedes, S. G. Massry, *Am. J. Nephrol.* **13**, 210 (1993).
7. M. Karperien *et al.*, *Mech. Dev.* **47**, 29 (1994).
8. K. Lee, J. D. Deeds, G. V. Segre, *Endocrinology* **136**, 453 (1995).
9. J. J. Orloff *et al.*, *Am. J. Physiol.* **262**, E599 (1992).
10. N. Inomata, M. Akiyama, N. Kubota, H. Jüppner, *Endocrinology* **136**, 4732 (1995).
11. S. Fukayama, A. H. Tashjian Jr., J. N. Davis, J. C. Chisholm, *Proc. Natl. Acad. Sci. U.S.A.* **92**, 10182 (1995).
12. T. B. Usdin, C. Gruber, T. I. Bonner, *J. Biol. Chem.* **270**, 15455 (1995).
13. A. van de Stolpe *et al.*, *J. Cell Biol.* **120**, 235 (1993).
14. A. C. Karaplis *et al.*, *Genes Dev.* **8**, 277 (1994).
15. N. Amizuka, H. Warshawsky, J. E. Henderson, D. Goltzman, A. C. Karaplis, *J. Cell Biol.* **126**, 1611 (1994).
16. A. Vortkamp, K. Lee, B. Lanske, G. V. Segre, H. M. Kronenberg, C. Tabin, *Science* **273**, XXX (1996).
17. M. R. Capecchi, *ibid.* **244**, 1288 (1989).
18. Two genomic clones (λ-8 and λ-15) were isolated from a λ-DASH II 129/SvJ mouse liver genomic library (1×10^7 plaque-forming units per milliliter) with the coding sequence of the rat PTH/PTHrP receptor as a probe (*4*, *27*). For construction of the targeting vector, a 4.5-kb Bam HI fragment containing exon E1 of the PTH/PTHrP receptor gene was used as the 5′ flanking region and subcloned by blunt end ligation into a similarly treated Xho I site in the pPNT plasmid (*14*). A 5.6-kb Eco RI fragment containing the 3′ untranslated region of the PTH/PTHrP receptor gene, cloned into the Eco RI polylinker site of pPNT, was used as the 3′ flanking region. The resulting targeting vector was linearized at the unique Not I site in the pPNT backbone for electroporation of ES cells. Double selection was carried out, and resistant ES clones were analyzed by Southern (DNA) blot analyses with an external intronic 0.9-kb Sac I–Xho I fragment at the 5′ end of the gene. Positive clones (12%) were injected into recipient blastocysts to generate chimeras as described (*28*). Progeny of two independent clones yielded the identical phenotype. All animal experimentation followed institutional guidelines.
19. B. Lanske *et al.*, data not shown.
20. Twenty-five embryos from E6.5 to E9.5 were examined histologically and had normal appearing Reichert's membrane. Five E9.5 embryos were examined by in situ hybridization for PTH/PTHrP receptor mRNA (*29*). The hybridization signal was strong in four embryos but was completely absent from one, a presumed PTH/PTHrP (−/−) fetus. Immunohistochemical staining was carried out on paraffin sections by standard techniques. Hybridization was done with a rabbit antibody to α-laminin (dilution, 1/300; Gibco). To increase the sensitivity, we used a second antibody specific for the first one (swine antibody to rabbit immunoglobulin G complex; DAKO). Visualization of this complex was obtained by hybridization with the ABComplex (horseradish peroxidase; DAKO).
21. M. Karperien, P. Lanser, S. W. de Laat, J. Boonstra, L. H. K. Defize, *Int. J. Dev. Biol.*, in press.
22. F. Beck, J. Tucci, P. V. Senior, *J. Reprod. Fertil.* **99**, 343 (1993).
23. M. McLeod, *Teratology* **22**, 299 (1980).
24. Fresh tissues were obtained by cesarean sections from fetuses derived from heterozygous interbreeding at day 18.5 of gestation. Fetuses were fixed in 10% formalin–phosphate-buffered saline (PBS) (pH 7.2) and subsequently decalcified in neutral 40% EDTA. Various parts of the skeleton were embedded in paraffin, and 5- to 10-μm-thick sections were stained with hematoxylin and eosin.
25. E. Schipani, K. Kruse, H. Jüppner, *Science* **268**, 98 (1995).
26. Hind limbs of E16.5 fetuses were severed at midfemur, stripped of skin, and then placed on a filter paper (pore size, 0.8 μm) on a wire mesh in a Falcon organ culture dish, and 1 ml of BGJ_b medium (Gibco BRL) was added. The hind limbs, which lay at the air-fluid interface, were cultured at 37°C in a humidified atmosphere of 95% air–5% CO_2 with daily changes of medium. The hind limbs were treated with either 10^{-7} M human PTHrP (1–34), recombinant murine Shh (5 μg/ml) (*16*), or vehicle (BGJ_b medium–0.1% bovine serum albumin) alone from day 2 for 4 days. The samples were never exposed to serum. At the termination of culture, the hind limbs were fixed in 10% formalin-PBS, paraffin-embedded, and cut in serial sections.
27. X. F. Kong *et al.*, *Biochem. Biophys. Res. Commun.* **200**, 1290 (1994).
28. A. Bradley, in *Teratocarcinomas and Embryonic Stem Cells: A Practical Approach*, E. Robertson, Ed. (IRL, Washington, DC, 1987), pp. 113–152.
29. Complementary ^{35}S- labeled RNA probes were transcribed from the rat PTH/PTHrP receptor cDNA (*4*) and from the human Ihh cDNA (*16*). In situ hybridization was done as described (*8*).

30. We thank C. Tabin for valuable collaboration and helpful reading of the manuscript, T. Doetschmann for reagents, E. Samson for technical assistance with histology, and M. Mannstadt for help and technical expertise. Supported by National Institutes of Health grants DK 47038 and DK 47237. B.L. was supported in part by a fellowship of the Max-Kade Foundation.

10 April 1996; accepted 20 June 1996

Emergence of Preferred Structures in a Simple Model of Protein Folding

Hao Li, Robert Helling,* Chao Tang,† Ned Wingreen

Protein structures in nature often exhibit a high degree of regularity (for example, secondary structure and tertiary symmetries) that is absent from random compact conformations. With the use of a simple lattice model of protein folding, it was demonstrated that structural regularities are related to high "designability" and evolutionary stability. The designability of each compact structure is measured by the number of sequences that can design the structure—that is, sequences that possess the structure as their nondegenerate ground state. Compact structures differ markedly in terms of their designability; highly designable structures emerge with a number of associated sequences much larger than the average. These highly designable structures possess "proteinlike" secondary structure and even tertiary symmetries. In addition, they are thermodynamically more stable than other structures. These results suggest that protein structures are selected in nature because they are readily designed and stable against mutations, and that such a selection simultaneously leads to thermodynamic stability.

Natural proteins fold into specific compact structures despite the huge number of possible configurations (*1*). For most single-domain proteins, the information coded in the amino acid sequence is sufficient to determine the three-dimensional (3D) folded structure, which is the minimum free-energy structure (*2*). Protein sequences must undergo selection so that they fold into unique 3D structures. Because folding maps sequences to structures, it is relevant to ask whether selection principles also apply to structures that have evolved in nature. Protein structures often exhibit a high degree of regularity—for example, secondary structures such as α helices and β sheets and tertiary symmetries—that is absent from random compact structures. What is the origin of these regularities? Does nature select special structures for design? What are the underlying principles that govern the selection of structures?

Here we describe results from a simple model of protein folding that suggest some answers to these questions. We focus on the properties of each individual compact structure by determining the sequences that have the given structure as their nondegenerate ground state. We show that the number of sequences (N_S) associated with a given structure (S) differs from structure to structure and that preferred structures emerge with N_S values much larger than the average. These preferred structures are "proteinlike," with secondary structures and symmetries, and are thermodynamically more stable than other structures.

Our results are derived from a minimal model of protein folding, which we believe captures the essential components of the

NEC Research Institute, 4 Independence Way, Princeton, NJ 08540, USA.

*Present address: Second Institute for Theoretical Physics, DESY/University of Hamburg, Hamburg, Germany. †To whom correspondence should be addressed. E-mail: tang@research.nj.nec.com